Properties of γ-decaying isomers and isomeric ratios in the ^{100}Sn region

J. Park,[1,2,*] R. Krücken,[1,2] D. Lubos,[3,4,5] R. Gernhäuser,[3] M. Lewitowicz,[6] S. Nishimura,[4] D. S. Ahn,[4] H. Baba,[4] B. Blank,[7] A. Blazhev,[8] P. Boutachkov,[9] F. Browne,[4,10] I. Čeliković,[6,11] G. de France,[6] P. Doornenbal,[4] T. Faestermann,[3,5] Y. Fang,[12] N. Fukuda,[4] J. Giovinazzo,[7] N. Goel,[9] M. Górska,[9] H. Grawe,[9] S. Ilieva,[13] N. Inabe,[4] T. Isobe,[4] A. Jungclaus,[14] D. Kameda,[4] G. D. Kim,[15] Y.-K. Kim,[15,16] I. Kojouharov,[9] T. Kubo,[4] N. Kurz,[9] G. Lorusso,[4] K. Moschner,[8] D. Murai,[4] I. Nishizuka,[17] Z. Patel,[4,18] M. M. Rajabali,[1] S. Rice,[4,18] H. Sakurai,[19] H. Schaffner,[9] Y. Shimizu,[4] L. Sinclair,[4,20] P.-A. Söderström,[4] K. Steiger,[3] T. Sumikama,[17] H. Suzuki,[4] H. Takeda,[4] Z. Wang,[1] H. Watanabe,[21] J. Wu,[4,22] and Z. Y. Xu[19]

[1]*TRIUMF, 4004 Wesbrook Mall, Vancouver, British Columbia, Canada V6T 2A3*

[2]*Department of Physics and Astronomy, University of British Columbia, Vancouver, British Columbia, Canada V6T 1Z1*

[3]*Physik Department, Technische Universität München, D-85748 Garching, Germany*

[4]*RIKEN Nishina Center, Wako-shi, Saitama 351-0198, Japan*

[5]*Excellence Cluster Universe, Technische Universität München, D-85748 Garching, Germany*

[6]*Grand Accélérateur National d'Ions Lourds (GANIL), CEA/DSM-CNRS/IN2P3, Boulevard H. Becquerel, 14076 Caen, France*

[7]*Centre d'Etudes Nucléaires de Bordeaux-Gradignan, 19 Chemin du Solarium, CS 10120, F-33175 Gradignan Cedex, France*

[8]*Institute of Nuclear Physics, University of Cologne, D-50937 Cologne, Germany*

[9]*GSI Helmholtzzentrum für Schwerionenforschung GmbH, D-64291 Darmstadt, Germany*

[10]*School of Computing, Engineering and Mathematics, University of Brighton, Brighton BN2 4GJ, United Kingdom*

[11]*Vinča Institue of Nuclear Sciences, University of Belgrade, 11000 Belgrade, Serbia*

[12]*Osaka University, Machikaneyama-machi 1-1, Osaka 560-0043 Toyonaka, Japan*

[13]*Technische Universität Darmstadt, D-64289 Darmstadt, Germany*

[14]*Instituto de Estructura de la Materia, IEM-CSIC, E-28006 Madrid, Spain*

[15]*Rare Isotope Science Project, Institute for Basic Science, Daejeon 305-811, Republic of Korea*

[16]*Department of Nuclear Engineering, Hanyang University, Seoul 133-791, Republic of Korea*

[17]*Department of Physics, Faculty of Science, Tohoku University, Sendai 980-0845, Japan*

[18]*Department of Physics, University of Surrey, Guildford GU2 7XH, United Kingdom*

[19]*University of Tokyo, 7-3-1 Hongo Bunkyo, Tokyo 113-0033, Japan*

[20]*University of York, York YO10 5DD, United Kingdom*

[21]*Beihang University, Beijing 100191, China*

[22]*Department of Physics, Peking University, Beijing 100871, China*

(Received 4 July 2017; published 9 October 2017; publisher error corrected 16 October 2017)

Half-lives and energies of γ rays emitted in the decay of isomeric states of nuclei in the vicinity of the doubly magic ^{100}Sn were measured in a decay spectroscopy experiment at Rikagaku Kenkyusho (The Institute of Physical and Chemical Research) of Japan Nishina Center. The measured half-lives, some with improved precision, are consistent with literature values. Three new results include a 55-keV $E2$ γ ray from a new (4^+) isomer with $T_{1/2} = 0.23(6)$ μs in ^{92}Rh, a 44-keV $E2$ γ ray from the (15^+) isomer in ^{96}Ag, and $T_{1/2}(6^+) = 13(2)$ ns in ^{98}Cd. Shell-model calculations of electromagnetic transition strengths in the $(p_{1/2}, g_{9/2})$ model space agree with the experimental results. In addition, experimental isomeric ratios were compared to the theoretical predictions derived with an abrasion-ablation model and the sharp cutoff model. The results agreed within a factor of 2 for most isomers. From the nonobservation of time-delayed γ rays in ^{100}Sn, new constraints on the $T_{1/2}$, γ-ray energy, and internal conversion coefficients are proposed for the hypothetical isomer in ^{100}Sn.

DOI: 10.1103/PhysRevC.96.044311

I. INTRODUCTION

The $N \sim Z$ region near ^{100}Sn is rich in nuclear structure phenomena while also being important for the astrophysical rapid-proton capture process. Among the relevant topics are the robustness of the $N = Z = 50$ shell closures in ^{100}Sn and the superallowed Gamow-Teller decay [1]; the limit of bound $N = Z$ heavy nuclei and the location of the proton dripline; the role of $T = 0$ proton-neutron (pn) interactions in contrast to the $T = 1$ seniority scheme in the $g_{9/2}$ orbit of $N = Z$ nuclei [2,3]; and masses, half-lives, and β-delayed proton emission branching ratios along the rp-process path [4,5]. A comprehensive review of the experimental and the theoretical endeavor in this region of the chart of nuclides is given in Refs. [6,7] and references therein.

Many of the topics listed above are manifest in numerous isomeric states of $N, Z \leqslant 50$ nuclei [7], which offer important insights into their structure: $E2$ seniority isomers in $N = 50$ isotones ^{92}Mo, ^{94}Ru, ^{96}Pd, and ^{98}Cd [8–11]; a high-spin, negative-parity isomer in ^{94}Pd [48] with $\ell = 1,3$ electric transitions ($E1$, $E3$); multiple isomers in ^{95}Ag [12] decaying via $\ell = 3,4$ electric transitions ($E3$, $E4$); $N = Z$ spin-gap

*Present address: Department of Physics, Lund University, Lund 22100, Sweden; joochun.park@nuclear.lu.se

isomers in ^{94}Ag, ^{96}Cd, and ^{98}In [3,13–19]; and core-excited isomers in ^{96}Ag and ^{98}Cd [20–22]. This is by no means an exhaustive list. Isomers decaying by γ-ray transitions with half-lives $T_{1/2}$ on the order of μs preserve the excited states for γ-ray spectroscopy in fragmentation and in-flight separation experiments. In addition to accessing the structure of nuclei below the isomers, properties of electromagnetic transitions can be used to determine experimental transition strengths $B(\sigma\ell; J_i^\pi \rightarrow J_f^\pi)$ for given multipolarities $\sigma\ell$ through which shell-model (SM) calculations [23–32] in the vicinity of ^{100}Sn can be scrutinized.

Properties of a few γ-decaying isomers in this region of nuclides are only partially known. For example, the (15^+) state in ^{96}Ag has been previously designated as isomeric with $T_{1/2} = 1.56(3)$ μs [20], but the transition energy to the (13^+) state has not been observed. An upper limit of 50 keV was placed on the electric quadrupole $E2$ γ-ray transition energy based on the isomer's $T_{1/2}$, supplemented by theoretical $B(E2)$ calculations. Another example is the (6^+) state in ^{98}Cd, predicted to be isomeric with $T_{1/2}$ ranging from 10 to 20 ns [11], for which the half-life analysis using $\gamma\gamma$ time differences with high-purity germanium (HPGe) detectors would be challenging owing to poor time resolutions at $E_\gamma < 200$ keV. The upper limit on the half-life of this (6^+) isomer was confirmed in Ref. [21].

As for ^{100}Sn, several different calculations have suggested an isomer decaying with a low-energy $E2$ transition with half-lives ranging from 90 ns to 2.6 μs: large-scale shell model (LSSM) with the Nowacki-Sieja interaction in the (g,d,s) model space [31,33] used in multiple works [1,3,17,20,21,30], SM-gd5 [32], and Hartree-Fock random particle approximation (HF-RPA) [34]. While the LSSM and the SM-gd5 calculations predict the isomer's spin to be 6^+, the HF-RPA calculation proposes an 8^+ isomer above the 6^+ state. $E2$ transition strengths of 0.7–1.1 W.u. and γ-ray energies between 80 and 260 keV were predicted by those calculations. With a significantly increased production rate, the hypothetical isomer and its cascade of γ rays may be observed experimentally to unveil the excited states of ^{100}Sn unless a direct proton emission branch (b_p) is much more favored.

II. EXPERIMENT AND ANALYSIS

^{100}Sn and nuclei with similar N and Z were produced by a fragmentation reaction of a 345 MeV/u ^{124}Xe primary beam on a 740 mg/cm^2 ^{9}Be target at the Rikagaku Kenkyusho (RIKEN, The Institute of Physical and Chemical Research) of Japan RI Beam Factory [35]. Isotopes of similar mass over charge ratios A/q and atomic number Z were separated at the first stage of BigRIPS by a $B\rho - \Delta E - B\rho$ method with a 3-mm Al wedge degrader, dipole magnets, and slits at the dispersive foci. The filtered beam was further separated and identified on an event-by-event basis by $B\rho - \mathrm{ToF} - \Delta E$ measurements at the later stages of BigRIPS and the ZeroDegree spectrometer [36,37] using position-sensitive parallel-plate avalanche counters [38], plastic scintillators, and an ionization chamber [39]. Figure 1 shows two regions of the particle identification plot, where contaminations in each identified nucleus were typically

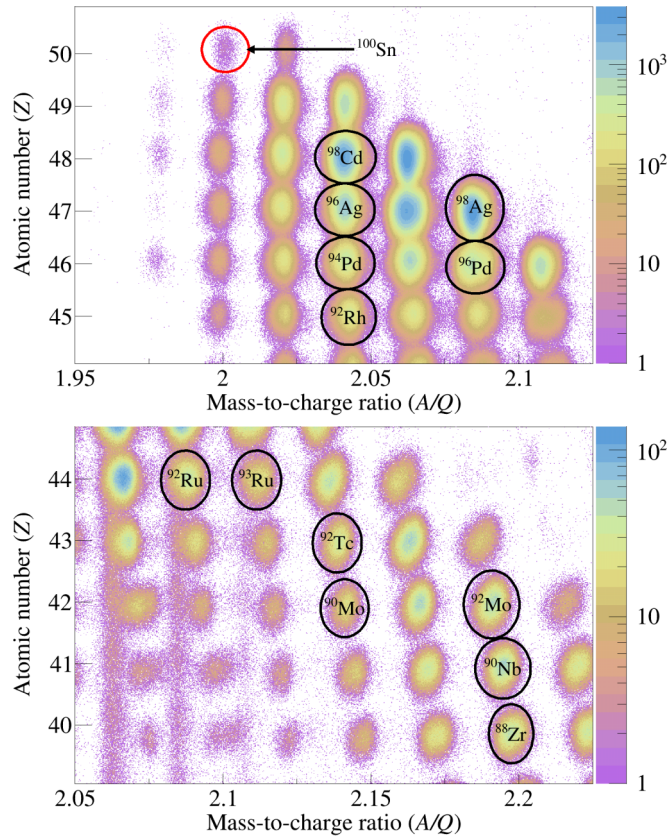

FIG. 1. Particle identification plots of nuclei produced in this experiment. Nuclei with isomeric γ-decay $T_{1/2}$ measurements listed in Table I are highlighted and labeled. The doubly magic ^{100}Sn is labeled as a reference.

below 1%. The flight time T_F through the separation and identification systems was calculated with LISE++ [40], where T_F in the rest frame of the ions ranged from 600 to 630 ns. This experiment has enabled the discovery of several new isotopes—^{90}Pd, ^{92}Ag, ^{94}Cd, and ^{96}In [41]—as well as the measurement of half-lives, β-decay endpoint energies, and β-delayed proton branching ratios of $N = Z - 1$ nuclei ^{91}Pd, ^{95}Cd, ^{97}In, and ^{99}Sn [42].

Ion implantation and particle decay (β, βp, p) measurements were carried out by the Wide-range Active Silicon Strip Stopper Array for Beta and Ion detection (WAS3ABi) [43]. The majority of the ions were implanted in the middle module of the three 1-mm-thick double-sided silicon strip detectors (DSSSDs) of WAS3ABi, where each DSSSD was segmented into 60×40 1-mm-wide strips in the x and y directions, respectively. Particle decay events were correlated to ion implantation events as described in Ref. [19], which used a similar set of segmented Si detectors. γ rays following decay events were detected with the Euroball-RIKEN Cluster Array (EURICA) [44], featuring a total of 84 HPGe crystals that surrounded WAS3ABi in a 4π geometry. During the experiment, 47 channels of EURICA were operational. The γ-ray time (T_γ) measurement window was set to 12 μs to detect isomeric γ rays with long-range time-to-digital converter (TDC) modules. The digital γ finder (DGF) modules

provided a longer time window up to 100 μs with better γ-ray detection efficiencies at low energies, but their time resolution was poorer compared to the TDC. The energy range of EURICA was $35 < E_\gamma$ (keV) < 6200. Internal conversion (IC) electrons associated with low-energy electromagnetic transitions could be measured with WAS3ABi only if the electron energies were well above the 100-keV software threshold cut and the half-life of the isomer was greater than the 600-μs dead time of WAS3ABi, during which the radioactive ion implantation event was read out by the data acquisition system.

With the help of high-resolution selection cuts in particle identification and characteristic γ-ray energies, the half-lives of γ-decaying isomers were measured with several methods. Most of the isomers presented in this work were populated before ion implantation, whose half-lives could be determined with the plastic scintillator trigger ($\sim$10-ps resolution) at the last focal plane of the ZeroDegree spectrometer as the start time (T_{start}) and the EURICA trigger as the stop time (T_{stop}). However, certain isomers were populated from the decays of parent isomers after implantation. If the parent isomer had a comparable or a longer half-life than the daughter, then the half-life of the daughter isomer was measured by fitting the $T_{\text{stop}} - T_{\text{start}}$ time difference distribution in $\gamma\gamma$ coincidence matrix. There were two instances of this scenario: the (8^+) and the (6^+) isomers in ^{98}Cd. However, if the parent isomer had a sufficiently shorter $T_{1/2}$ than the daughter, then the time distribution of the γ rays depopulating the daughter was fit with a sufficiently delayed time window to attenuate the feeding from the parent isomer. This was the case for the 14^+ isomer in ^{94}Pd and the (15^+) isomer in ^{96}Ag. The half-life of the isomer in ^{98}Ag was determined by fitting the time distribution of the 107-keV γ ray emitted after the β decay of ^{98}Cd rather than the isomeric decay of ^{98}Ag for higher statistics. In this case the start time trigger was provided by WAS3ABi, and the γ rays feeding the isomer were assumed to be prompt.

After setting energy gates on γ-ray energy peaks belonging to the decay cascade of the isomer, the γ-ray time distribution was fitted with an exponentially modified Gaussian. The Gaussian component characterized the energy-dependent time jitter of the TDC and DGF modules, where the time resolution was typically less than 20 and 40 ns, respectively. Unbinned maximum likelihood (MLH) methods were used to determine the half-lives with the exception of the (4^+) isomer in ^{98}Ag, on which the binned χ^2 method was applied. This was attributable to the necessary background subtractions of randomly correlated β decays of the parent nucleus ^{98}Cd. The probability density function contained the main decay component and the background time profile deduced from γ-ray energy gates on the sides of the peaks of interest. Following $T_{1/2}$ and E_γ measurements, experimental $B(\sigma\ell; J_i^\pi \rightarrow J_f^\pi)$ were determined with branching ratios and IC coefficients α. In this work, α was obtained using the software BRICC [45].

Experimental isomeric ratios R_{exp} as defined in Ref. [46] were determined for a majority of isomers in the ^{100}Sn region, including those that decay by particle emission. The mathematical expression for R_{exp} is

$$R_{\text{exp}} = \frac{I_{\text{abs}}}{N_{\text{imp}} \Pi_i \epsilon_i}, \quad (1)$$

where I_{abs} is the absolute intensity of the isomeric decay, N_{imp} is the number of implanted nuclei, and $0 < \epsilon_i < 1$ are various correction factors which depend on the decay mode. For γ-decaying isomers, ϵ_i originate from losses during the flight time through the separator and the finite T_γ window of 12 μs. For all other types of isomeric decays ϵ_i are decay correlation efficiencies, WAS3ABi dead-time correction factors, and normalization factors owing to finite time windows for the decay correlation.

III. RESULTS AND DISCUSSION

A. Half-lives and transition strengths of the known isomers

Previously measured half-lives of γ-decaying isomeric states in proton-rich Zr, Nb, Mo, Tc, Ru, Pd, Ag, and Cd nuclei were remeasured from this data set. The plots of γ-ray decay curve analyses are presented in Fig. 2, and the properties of the isomers (including new measurements) are summarized in Table I. The list is not exhaustive, as only the transitions with sufficient statistics and 10 ns $< T_{1/2} <$ 10 μs were measured. The half-lives determined from this experiment are consistent with the NUBASE2016 values [47], but significant deviations have been observed for the following isomers: the 14^+ isomer in ^{94}Pd, the (4^+) isomer in ^{98}Ag, and the (8^+) isomer in ^{98}Cd. Though not as severe, the discrepancy in the half-lives of the 8^+ isomer in ^{96}Pd was 2σ. In all four cases, the half-lives determined from this experiment are smaller than those in Ref. [47], but consistent with other literature values [10,21,48–52]. One publication [53], reports consistently longer half-lives for these isomers, possibly pointing towards some systematic effect in that analysis. Thus, new weighted averages of literature half-lives were calculated after excluding the $T_{1/2}$ values in Ref. [53]. A good agreement in $T_{1/2}$ was achieved for all four isomers between the revised literature and this work.

To compare experimental isomeric $E2$ transitions within the ^{100}Sn core to theoretical predictions, SM calculations were performed with the code NUSHELLX [54] with the single-particle energies (SPEs) and two-body matrix elements (TBMEs) derived by Serduke, Lawson, and Gloeckner (SLG) [23] in the $\pi\nu(p_{1/2}, g_{9/2})$ model space (pg) for both protons (π) and neutrons (ν) with a ^{76}Sr core. In particular, the SPE and TBME based on a seniority-fit total-energy scheme (SLGM) found in the NUSHELLX package were used. Two sets of effective charges were used to calculate the theoretical $B(E2)$: $e_p = 1.5\ e$, $e_n = 0.5\ e$ (a) being the standard for large model spaces and $e_p = 1.72\ e$, $e_n = 1.44\ e$ (b), which has been tuned for proton-rich $A \sim 90$ nuclei in the small pg model space [55]. The results are listed in Table I, along with additional $B(\sigma\ell)$ values from other interactions and model spaces. Figure 3 shows graphical comparisons of experimental/theoretical transition strengths, which agree generally within different sets of interactions and effective charges. Notable differences were found for the isomers in ^{92,93}Ru, and the core-excited (12^+) isomer in ^{98}Cd.

B. A new (4^+) isomer in ^{92}Rh

Following ^{92}Rh implantation, a new time-delayed γ-ray transition was observed at 55.3(3) keV, as shown in Fig. 4. An

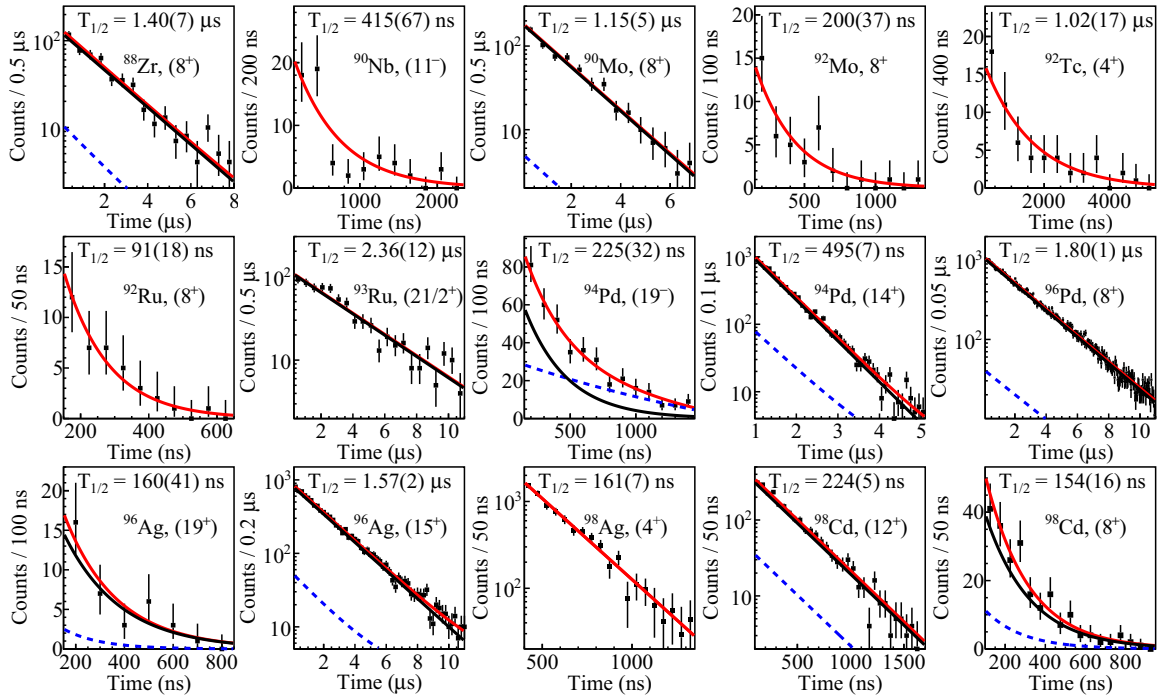

FIG. 2. Energy-gated γ-ray time distributions and half-lives of known isomers in the ^{100}Sn region, having $T_{1/2} < 10$ μs. The full fit functions (solid red line) contain the signal (solid black line) and the background (dashed blue line) components.

unbinned MLH fit of the time distribution of the events in this energy peak yielded $T_{1/2} = 0.23(6)$ μs. The newly measured transition energy and the half-life are similar to the 54.6(2)-keV $E2$ transition from the (2^+) isomer to the (4^+) ground state in ^{94}Rh, with a half-life of 0.48(4) μs [56].

Because the 55-keV γ ray does not correspond to any of the known transitions or energy gaps in ^{92}Rh, a new isomeric state is proposed. Given only one time-delayed γ ray, the isomer should lie 55 keV above any of the two near-degenerate β-decaying states with the given spins: $(\geqslant 6^+)$ or (2^+) [57]. To examine low-energy states in this nucleus not unveiled by previous experiments [16,58,59], SM calculations of the low-energy states of ^{92}Rh were performed (see Fig. 5). The SLGM interaction reproduces the two lowest-lying states and the excitation energy of the low-lying (8^+) state in ^{92}Rh. A 4^+ state is predicted above the 2^+ and the 6^+ states with energy differences of 71 and 36 keV, respectively, and other low-energy states are predicted at least 150 keV above the ground state.

The similarity in excitation energy was supplemented by the transition strength comparison, where three pure multipolarities were assumed for the 55-keV γ ray: $E1$, $M1$, and $E2$. Higher multipolarities would correspond to unphysical transition strengths based on the experimental half-life, the γ-ray energy, and the corresponding IC coefficient. According to the SM results shown in Fig. 5, an $E1$ transition with $E_\gamma \approx$ 200 keV is possible from the 4^- state to the 4^+ state. However, the predicted energy difference between the two states is rather large compared to the experimental γ-ray energy. $M1$ transitions may originate from a 1^+ state or a 7^+ state, but the experimental $B(M1)$ value of $9.7(25) \times 10^{-6}$ W.u. is much smaller than the theoretical predictions.

Alternatively, the experimental $B(E2) = 15.8(42)$ W.u. is compatible with the theoretical $B(E2)$ from the 4^+ state to the 2^+ state using either of the effective charge sets (a) or (b). The SLGM interaction predicts a much smaller $E2$ strength to the 6^+ state, so the (2^+) state was tentatively assigned as the final state. Owing to low statistics, tagging the implanted ^{92}Rh nuclei with the 55-keV isomeric γ ray and measuring the β-decay half-life to determine the final state was not conclusive. In either case, there is sufficient evidence to suggest the existence of a (4^+) isomer in ^{92}Rh with an $E2$ transition. Furthermore, this conclusion agrees well with results based on the Gross-Frenkel (GF) interaction in the pg model space [24].

C. Transition energy of the (15^+) isomer in ^{96}Ag

The transition energy from the (15^+) isomer to the (13^+) state in ^{96}Ag was measured for the first time, which has been postulated to be <50 keV [20]. Figure 6 shows a time-delayed γ-ray spectrum with a peak at 43.7(2) keV, with signatures of $\gamma\gamma$ coincidence relation with the known 667-keV γ ray depopulating the (13^+) state. A decay curve analysis of the time distribution of the 44-keV γ ray yielded a half-life of 1.48(27) μs, which is consistent with both 1.543(28) μs [47] and 1.55(3) μs deduced in this work using the 630- and 667-keV γ rays that belong to the isomer's decay cascade [20]. A γ-ray intensity analysis using the efficiency of EURICA yielded $\alpha = 33(6)$, which is consistent with the BRICC value of 27.9(7) [45].

The γ-ray energy measurement enables the comparison of the experimental $E2$ transition strength to SM predictions. From $\Delta E = 43.7(2)$ keV, $\alpha = 27.9(7)$ and a weighted average $T_{1/2} = 1.546(20)$ μs, the experimental $B(E2)$ value is

TABLE I. γ-decaying isomers with measured half-lives. Isomeric decay information (excitation/transition energy, total internal conversion coefficient α calculated from BRICC [45], branching ratios, and multipolarity $\sigma\ell$) is given. Literature $T_{1/2}$ values are taken from NUBASE2016 [47] unless otherwise specified. Weighted averages of half-lives obtained from this work and the literature were used to calculate experimental transition strengths. For $E2$ transitions in the pg model space, SM calculations with the NUSHELLX code [54] with the SLGM interaction [23] are listed with two sets of effective charges: (a) $e_p = 1.5\ e$, $e_n = 0.5\ e$ and (b) $e_p = 1.72\ e$, $e_n = 1.44\ e$. Theoretical transition strengths calculated with other model spaces and interactions are also listed.

Nucleus	$T_{1/2}$ (μs)		E_γ (keV)	α	BR(%)	$\sigma\ell; J_i^\pi \rightarrow J_f^\pi$	$B(\sigma\ell)$/W.u.		
	This work	Literature			(with IC)		Exp	(a)	(b)
^{88}Zr	1.40(7)	1.320(25)	77	2.87(4)	100	$E2; 8^+ \rightarrow 6^+$	1.75(4)	0.55	2.40
^{90}Nb	0.415(67)	0.472(13)	1067	$<10^{-2}$	73(7)	$M2; (11^-) \rightarrow (9^+)$	$8.6(7)\times10^{-5}$		
			71	3.97(6)	27(7)	$E2; (11^-) \rightarrow (9^-)$	1.50(29)	1.92	2.59
^{90}Mo	1.15(5)	1.12(5)	63	6.30(9)	100	$E2; 8^+ \rightarrow 6^+$	2.84(10)	1.63	4.00
^{92}Mo	0.200(37)	0.190(3)	148	0.291(4)	100	$E2; 8^+ \rightarrow 6^+$	1.31(2)	1.12	1.48
^{92}Tc	1.02(17)	1.03(7)	56	9.79(14)	100	$E2; (4^+) \rightarrow (6^+)$	3.64(23)	1.37	4.81
^{92}Ru	0.091(18)	0.100(14)	163	0.225(4)	100	$E2; (8^+) \rightarrow (6^+)$	1.67(19)	4.54	9.43
^{92}Rh	0.23(6)		55.3(3)	11.2(2)	100	$E2; (4^+) \rightarrow (2^+)$	15.8(42)	7.4	18.3
^{93}Ru	2.36(12)	2.27(17)	146	0.331(5)	100	$E2; (21/2^+) \rightarrow (17/2^+)$	0.109(6)	0.455	0.596
^{94}Pd	0.225(32)	0.197(22)	1651	$<10^{-2}$	80(4)	$E3; (19^-) \rightarrow (16^+)$	0.28(3)	0.10[a]	0.18[a]
			106	0.129(2)	20(4)	$E1; (19^-) \rightarrow (18^+)$	$2.5(5)\times10^{-7}$		
	0.495(7)	0.489(11)[b]	96	1.65(2)	100	$E2; 14^+ \rightarrow 12^+$	2.16(7)	1.43	3.30
								2.69[a]	5.49[a]
^{96}Pd	1.80(1)	1.76(4)[c]	106	1.11(2)	100	$E2; (8^+) \rightarrow (6^+)$	0.417(4)	0.249	0.327
^{96}Ag	0.160(41)	0.16(3)	4265	$<10^{-2}$	19(9)	$E4; (19^+) \rightarrow (15^+)$	0.9(4)	0.7[d]	
			98	1.55(2)	81(9)	$E2; (19^+) \rightarrow (17^+)$	4.7(8)	3.57[d]	
	1.57(2)	1.543(28)	43.7(2)	27.9(7)	100	$E2; (15^+) \rightarrow (13^+)$	3.04(11)	2.99	4.27
								3.83[d]	
^{98}Ag	0.161(7)	0.154(8)[e]	107	1.12(2)	100	$E2; (4^+) \rightarrow (6^+)$	4.47(15)	1.69[f]	4.75[f]
^{98}Cd	0.224(5)	0.24(4)	4207	$<10^{-2}$	88(2)	$E4; (12^+) \rightarrow (8^+)$	3.03(8)	0.77[g]	
			49.2(2)	18.9(3)	12(2)	$E2; (12^+) \rightarrow (10^+)$	1.99(25)	0.72[g]	
	0.154(16)	$0.17^{+0.06}_{-0.04}$[h]	147	0.377(6)	100	$E2; (8^+) \rightarrow (6^+)$	1.42(14)	1.46	1.91
								2.12[g]	
	0.013(2)	<0.020	198	0.133(2)	100	$E2; (6^+) \rightarrow (4^+)$	4.7(7)	3.6	4.8
								5.35[g]	

[a]From SM calculations in the $\pi\nu(f_{5/2},p,g_{9/2})$ model space, reported in Ref. [48].
[b]Weighted average from Refs. [48,49].
[c]Weighted average from Refs. [10,49,50].
[d]From LSSM calculations in the $\pi\nu(g,d,s)$ model space, reported in Ref. [20].
[e]Weighted average from Refs. [51,52].
[f]Based on the SR88MHJM interaction [6,32] in the $\pi(p_{1/2},g_{9/2})\nu(g_{7/2},d,s,h_{11/2})$ model space, reported in Ref. [52].
[g]From LSSM calculations [33] in the $\pi\nu(g,d,s)$ model space, allowing up to five particle-hole excitations ($t = 5$).
[h]From Ref. [21].

3.04(11) W.u. The $B(E2)$ value agrees very well with the predictions with standard effective charges (a) based on SLGM interactions, and also with GF interactions in the same pg model space [20] that both yield $B(E2) = 2.99$ W.u. However, $B(E2) = 4.27$ W.u. when enhanced effective charges (b) are employed. This overestimation of the $B(E2)$ can be explained by the fact that the wave function of the (15^+) isomer is a fully stretched configuration of three-proton and one-neutron holes in the $g_{9/2}$ orbit. Enhanced effective charges account for nucleon excitations in the $p_{3/2}$ and $f_{5/2}$ orbits that cannot be calculated in the reduced pg model space, but the (15^+) isomer is a pure state composed of $g_{9/2}$ holes and thus requires no extra compensation. This argument is supported by the negligible difference in the calculated $B(E2)$ value in the extended $f_{5/2},p,g_{9/2}$ model space [48], as reported in Ref. [20]. When the gds model space and the interaction parameters provided in Refs. [60,61] are used, the $B(E2)$ value of this isomeric transition is slightly overestimated at 3.83 W.u. [20]. Therefore, core excitation is suggested to be negligible for the (15^+) isomer in ^{96}Ag. A similar phenomenon occurs with the (8^+) isomer in ^{98}Cd, which is a fully stretched configuration of two proton holes in the $g_{9/2}$ orbit. Based on $T_{1/2} = 149(14)$ ns measured in this work, $B[E2; (8^+) \rightarrow (6^+)] = 1.48(14)$ W.u. agrees better with 1.46 W.u. calculated with (a) than 1.91 W.u. from (b).

D. Low-spin states in ^{98}Ag

The half-life of the isomer in ^{98}Ag was measured to be 160(7) ns with a gate on the delayed 107-keV γ ray, which is consistent with the following literature values: 160(10) ns [51], and 142(13) and 158(26) ns [52]. In addition, those

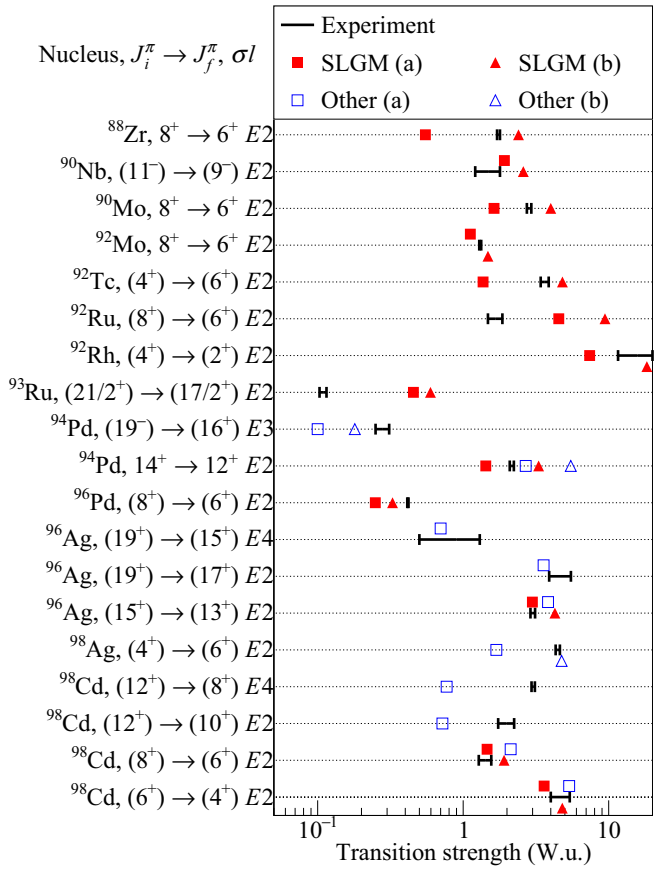

FIG. 3. Comparisons between experimental and theoretical transition strengths listed in Table I, where the SLGM interaction, and effective charge sets (a) and (b) are described in Sec. III A. For the calculated values labeled as "Other," see the footnotes in Table I.

previous works have proposed a reversed order of the 107- and 61-keV γ-ray transitions compared to the literature level scheme of the low-lying states of ^{98}Ag [62]. Concordantly,

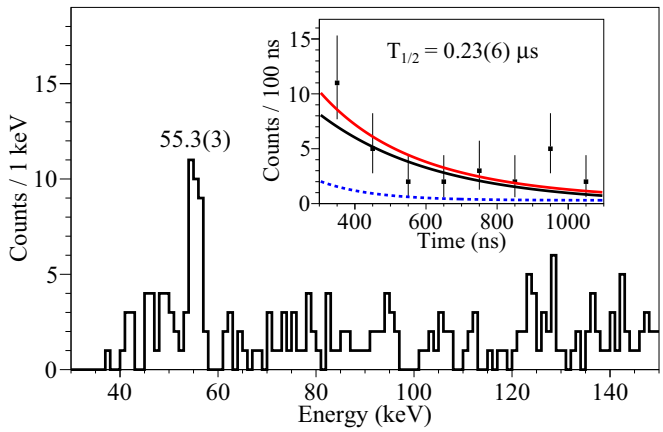

FIG. 4. γ-ray energy spectrum between 300 and 1200 ns after ^{92}Rh implantation. The inset shows the time distribution of the 55.3(3)-keV γ ray (background component as a dashed blue line) and the corresponding $T_{1/2}$.

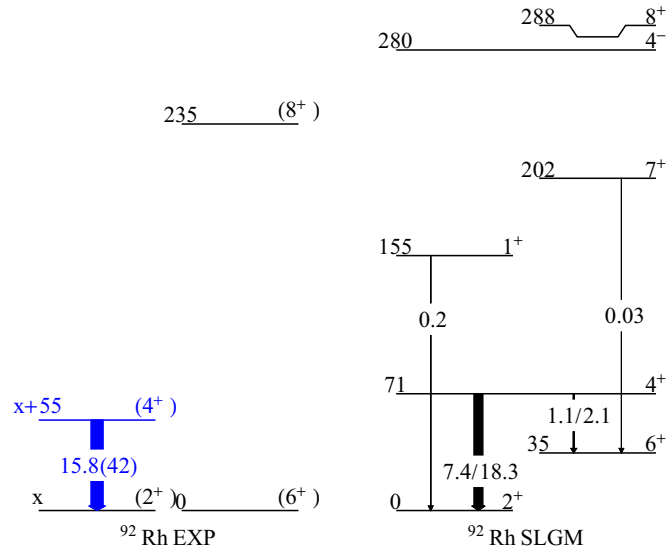

FIG. 5. Experimental and theoretical level schemes of low-energy states in ^{92}Rh. γ-ray transitions are labeled with their theoretical $B(E2)$ values in Weisskopf units, which were calculated with two sets of effective charges: $(e_p = 1.5e, e_n = 0.5e)$ and $(e_p = 1.72e, e_n = 1.44e)$, respectively.

the absence of delayed 61-keV γ rays in this work suggests a placement of the 61-keV transition above the 107 keV with appropriate changes in spin assignments (see Fig. 7) to comply with $\sigma\ell$ values previously determined from comparisons of IC coefficients [63]. The revised level scheme was presented in previous works [51,52] supported by SM calculations employing the "SR88MHJM" interaction [6,32]; this model includes final monopole corrections to the "SR88MHJ" interaction [64], and was used to calculate the $B(E2)$ value of the 107-keV transition.

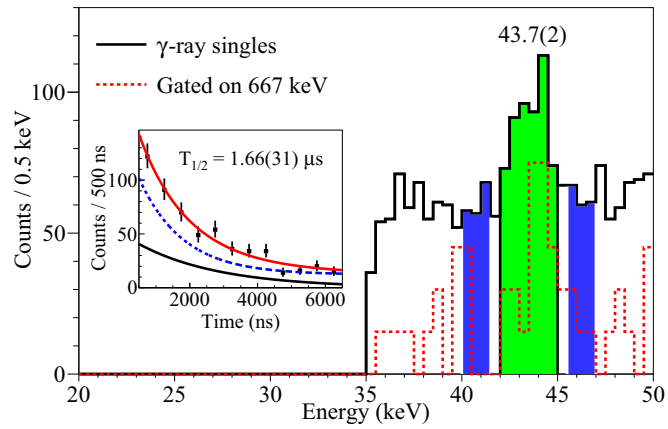

FIG. 6. γ-ray energy spectrum of ^{96}Ag for $500 < T_\gamma(\text{ns}) < 6500$ after implantation. The energy gates for the $T_{1/2}$ analysis are shown as green (total) and blue (background) histogram bins. Dashed red, γ-ray coincidence projection gated by the 667-keV transition from the (13^+) state in ^{96}Ag, whose counts were multiplied by 15 for comparison. The inset shows a γ-ray time spectrum of the 44-keV peak and the deduced $T_{1/2}$ value, which is consistent with both 1.543(28) μs [47] and 1.57(2) μs measured in this work.

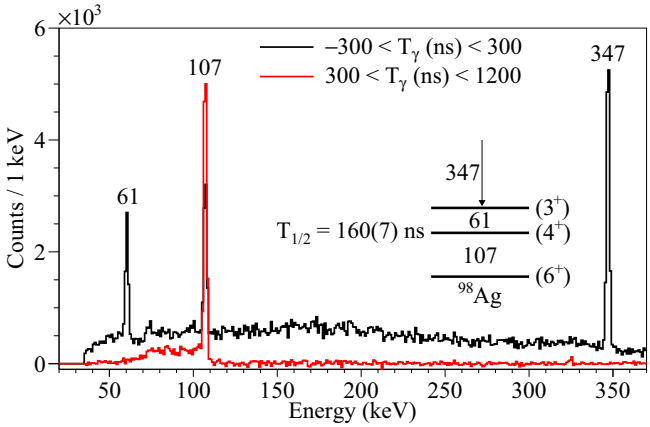

FIG. 7. Black histogram, prompt γ-ray spectrum of ^{98}Ag, generated from the β-decay of ^{98}Cd. The counts were scaled down to 1/5 of the original values for comparison. Red histogram, time-delayed γ-ray spectrum from the same β-decay data. The inset shows a partial level scheme of ^{98}Ag suggested previously in Refs. [51,52], which agree with the results of this work.

E. Half-life of the (6^+) isomer in ^{98}Cd

Previously constrained as $T_{1/2} < 20$ ns [21], the half-life of the (6^+) state in ^{98}Cd was measured by fitting the $\gamma\gamma$ time difference distribution of a 147-keV transition populating the (6^+) state and any of the 198/688/1395-keV transitions below the (6^+) state. From this procedure, the order of the 147- and 198-keV transitions in the seniority scheme of this nucleus was confirmed for the first time. The time difference distribution featured a decay curve with a $\sigma \approx 10$ ns EURICA time resolution, which could be fitted with an exponentially modified Gaussian. As shown in Fig. 8, adding 688- and 1395-keV transitions in the coincidence condition was justified

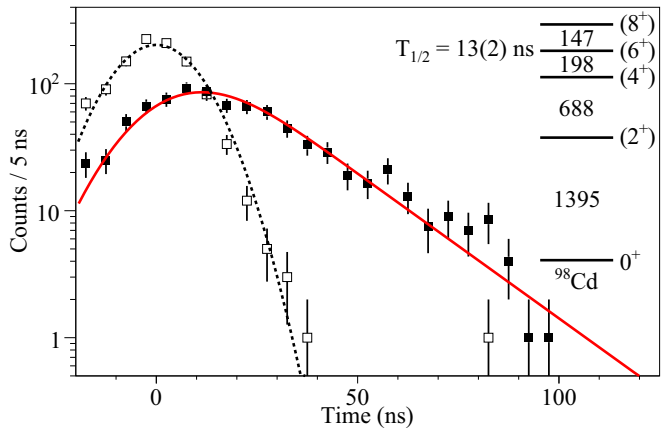

FIG. 8. Open squares, γ-ray time difference distribution of 198 keV (start) and 688/1395 keV (stop), which features only a Gaussian time jitter of the TDC; filled squares, γ-ray time difference distribution of 147 keV (start) and 198/688/1395 keV (stop), which exhibits an exponential decay component. The half-life of the (6^+) state in ^{98}Cd was determined to be 13(2) ns from the decay curve analysis.

by the prompt half-lives of the (2^+) and the (4^+) states. The resulting $T_{1/2} = 13(2)$ ns was combined with $\alpha = 0.133(2)$ for the 198-keV $E2$ γ ray to yield $B[E2;(6^+) \rightarrow (4^+)] = 4.7(7)$ W.u. The experimental $B(E2)$ value agrees well with the theoretical value obtained from SLGM interactions with enhanced effective charges (b), which is 4.8 W.u. However, within 2σ uncertainty the theoretical $B(E2) = 3.6$ W.u. calculated with standard effective charges (a) is also consistent. LSSM calculations based on the Nowacki-Sieja interaction [33] in the extended $\pi\nu(g_{7/2},d,s)$ model space with up to four particle-hole (p-h) excitations were also performed [21]. The resultant $B(E2)$ value of 5.13 W.u. based on the standard effective charges (a) is in great agreement with the experimental value. However, the $B[E2;(8^+) \rightarrow (6^+)]$ value was slightly overestimated at 2.03 W.u. from the LSSM calculations. Similar results were obtained from allowing up to five p-h excitations, as shown in Table I.

F. Comparison of experimental isomeric ratios to theory

The experimental isomeric ratios $R_{\rm exp}$ were compared to theoretical predictions $R_{\rm theo}$ as described in other experimental literature with various primary beam energies and projectile masses of fragmentation reactions [46,65,66]. The initial step of the theoretical calculations involves the final spin distribution of the fragments. The statistical abrasion-ablation model [67] was adopted to generate a probability density function in terms of the fragment's spin J [68],

$$P_J = \frac{2J+1}{2\sigma_f^2} e^{-J(J+1)/2\sigma_f^2}, \tag{2}$$

where σ_f is the spin cutoff parameter of the final fragment:

$$\sigma_f^2 = \langle j_z^2 \rangle \frac{(A_p - A_f)(\nu A_p + A_f)}{(\nu+1)^2(A_p - 1)}. \tag{3}$$

The first term $\langle j_z^2 \rangle$ is the average square of the spin projection of each nucleon in the fragment and is calculated based on the semiclassical treatment of the angular momentum distribution in the Woods-Saxon potential,

$$\langle j_z^2 \rangle = 0.16 A_p^{2/3} \left(1 - \tfrac{2}{3}\beta\right), \tag{4}$$

where β is the quadrupole deformation parameter of the fragmented nucleus. Negligible deformations are expected for nuclei in the vicinity of the doubly magic ^{100}Sn, so $\beta = 0$ was assumed in this work. $A_p = 124$ is the projectile nucleus's mass number (^{124}Xe primary beam), and A_f is the fragment nucleus's mass number. The parameter ν is the mean number of evaporated nucleons per abrasion of one nucleon which varied depending on the projectile nuclei and the primary beam energy. $\nu = 2$ was assumed for primary beams of 750 MeV/u ^{238}U [66] and 1 GeV/u ^{208}Pb, while $\nu = 0.5$ was used for a 60 MeV/u ^{92}Mo beam [65]. In comparison to the cited works, the 345-MeV ^{124}Xe beam used in this experiment has intermediate quantities in both mass and energy. Several values of ν were used to calculate different sets of $R_{\rm theo}$.

After having determined the formulas to calculate the distribution of J, the sharp cutoff model (SCM) was employed. For a given isomeric state with spin J_m, the SCM assumes

TABLE II. Isomeric ratios of nuclei determined in this work. Three different sets of theoretical isomeric ratios were calculated for each ν (mean number of evaporated nucleons per abrasion of one nucleon), and the standard deviations to $R_{\rm exp}$ for $J > 4$ positive-parity isomers are given for comparison.

Nucleus	J^π_m	Decay mode(s)	$R_{\rm exp}$ (%)	$R_{\rm theo}$ (%)		
				$\nu = 0.5$	$\nu = 1$	$\nu = 2$
^{88}Zr	(8^+)	γ, IC	69(5)	63	56	44
^{90}Nb	(11^-)	γ, IC	16(3)	41	33	20
^{90}Mo	(8^+)	γ, IC	61(3)	62	55	42
^{90}Rh	(7^+)	β, βp	86(3)	69	63	51
^{91}Nb	$(17/2^-)$	γ, IC	47(12)	58	50	37
^{92}Mo	(8^+)	γ, IC	48(10)	61	53	41
^{92}Tc	(4^+)	γ, IC	10(1)	87	84	78
^{92}Ru	(8^+)	γ, IC	32(33)	61	54	41
^{92}Rh	(4^+)	γ, IC	6.8(32)	87	83	77
^{93}Tc	$(17/2^-)$	γ, IC	54(5)	55	47	34
^{93}Ru	$(21/2^+)$	γ, IC	53(2)	42	33	20
^{94}Ru	8^+	γ, IC	68(6)	58	50	37
^{94}Pd	(19^-)	γ, IC	6.8(29)	5.9	2.8	0.6
	(14^+)	γ, IC	30(1)	21	14	5.8
^{94}Ag	(7^+)	β, βp	77(3)	66	58	46
	(21^+)	β, βp, p	<3	3.2	1.3	0.2
^{95}Pd	$(21/2^+)$	β	77(11)	40	31	18
^{95}Ag	$(37/2^+)$	γ, IC	7.7(7)	11	6.0	1.8
	$(23/2^+)$	γ, IC	41(7)	33	25	13
	$(1/2^-)$	γ, IC	2.9(8)	99	99	99
^{96}Pd	(8^+)	γ, IC	76(1)	56	48	34
^{96}Ag	(19^+)	γ, IC	1.4(8)	5.0	2.2	0.4
	(15^+)	γ, IC	18.7(4)	15	9.0	3.1
	(13^-)	γ, IC	12.4(13)	24	16	7.4
	(2^+)	β, βp	22(3)	95	94	92
^{96}Cd	(16^+)	β, βp	22(3)	12	6.5	2.0
^{97}Cd	$(25/2^+)$	β, βp	37(3)	25	17	8.0
^{98}Ag	(4^+)	γ, IC	4.2(10)	85	81	73
^{98}Cd	(12^+)	γ, IC	10(1)	27	19	9.0
	(8^+)	γ, IC	97(36)	54	45	32
^{98}In	(9^+)	β, βp	59(2)	47	38	25
		$\sigma(J^+_m > 4$ only)		18.1	23.2	32.3

that only the states with $J > J_m$ undergo spin-decreasing electromagnetic transitions to populate the isomer. A possible underestimation of the isomeric ratio of the SCM is offset by another crude assumption that all of the transitions from $J > J_m$ states are funneled to the isomer. Then $R_{\rm theo}$ is given by

$$R_{\rm theo} = \int_{J_m}^{\infty} P_J dJ = e^{-J_m(J_m+1)/2\sigma_f^2}, \quad (5)$$

with σ_f^2 given in Eq. (3).

Table II lists the isomers' J^π_m, decay mode(s), $R_{\rm exp}$ and $R_{\rm theo}$ calculated with $\nu = 0.5$, 1, and 2. $R_{\rm theo}$ calculated with $\nu = 0.5$ resulted in the best agreement with $R_{\rm exp}$, and the corresponding $R_{\rm exp}/R_{\rm theo}$ ratios are plotted in Fig. 9. For positive-parity isomers with $J^+_m > 4$, all of the ratios lie between 0.5 and 2. For $J^\pi_m \leqslant 4$, the SCM breaks down because

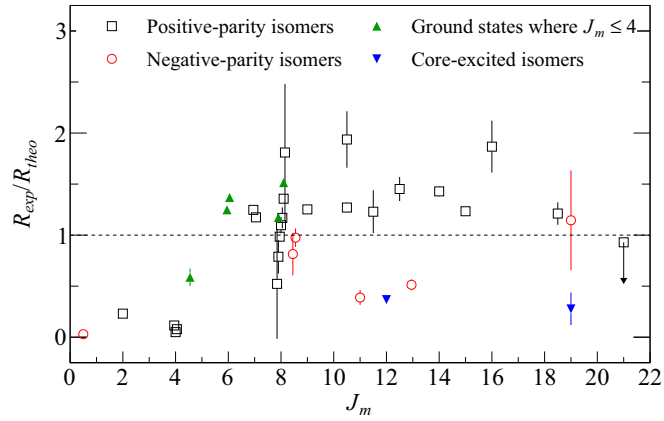

FIG. 9. Comparisons between experimental and theoretical isomeric ratios of nuclei in the ^{100}Sn region. The theoretical isomeric ratios used in this plot were determined from the sharp cutoff model with $\nu = 0.5$.

the isomers' spins are lower than the corresponding ground-state spins. In such cases, the population fractions of the ground states were compared to $R_{\rm theo}$. They also demonstrate agreement within a factor of 2. For negative-parity isomers, two experimental fractions are lower than the predicted values: the (11^-) isomer in ^{90}Nb and the (13^-) isomer in ^{96}Ag. No trivial explanation exists at the moment for the low $R_{\rm exp}$ in ^{90}Nb. For ^{96}Ag, however, higher-energy isomers with $J^\pi_m = (15^+)$ and (19^+) siphon some of the feeding to the (13^-) isomer. When the upper limit of the integral in Eq. (5) was modified to $J = 15$, $R_{\rm theo} = 9.5\%$, a much better agreement with $R_{\rm exp} = 12.4(13)\%$. Finally, two core-excited isomers report low $R_{\rm exp}/R_{\rm theo}$ ratios: the (19^+) isomer in ^{96}Ag and the (12^+) isomer in ^{98}Cd. The reason for this phenomenon is attributed to the need to knock out a nucleon from the ^{100}Sn core, which is more bound than a nucleon above the $N = Z = 50$ shell by 4–5 MeV.

G. Properties of the hypothetical $E2$ isomer in ^{100}Sn

A search for a core-excited isomer decaying by an $E2$ transition in ^{100}Sn [6] was carried out, but time-delayed γ rays were not observed in this nucleus. Owing to the high excitation energy, this hypothetical isomer may also possess a nonzero b_p with a half-life well below the 600-μs dead time of WAS3ABi. The β-decay analysis of ^{100}Sn with limited statistics did not yield a clear signature of ^{99}In. In this work, an upper limit on the half-life of an isomer assumed to decay by an $E2$ γ ray and $b_p = 0$ is proposed based on the expression

$$T_{1/2} < \frac{\ln(2) T_F}{H[\ln(\epsilon N_{\rm ion} R) - \ln(N_\gamma H)]}, \quad (6)$$

where T_F is the flight time of the ^{100}Sn ions through the separator, ϵ is EURICA's detection efficiency, $N_{\rm ion}$ is the number of implanted ^{100}Sn nuclei, R is the isomeric ratio, N_γ is the number of available γ rays for observation, and $H = 1 + \alpha$ is the hindrance factor for electromagnetic decays

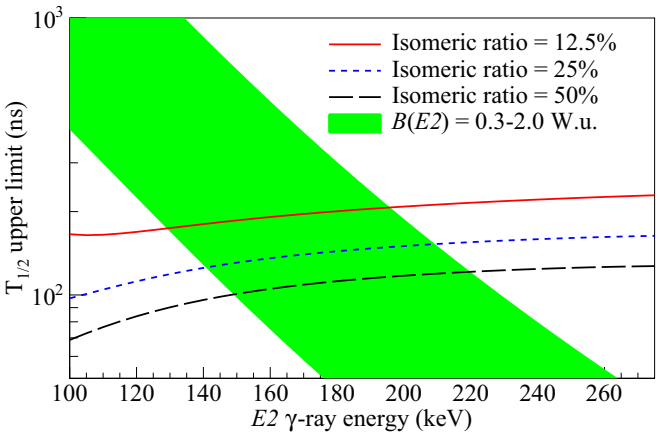

FIG. 10. Upper limits on the half-life of a hypothetical $E2$ isomer in ^{100}Sn as a function of γ-ray energy and three different isomeric ratios. The green band displays the relationship between $T_{1/2}$ and E_γ for $B(E2) = 0.3-2.0$ W.u. Conservative limits of $E_\gamma > 125$ keV and $T_{1/2} < 210$ ns are deduced for ^{100}Sn's isomer, assuming $R = 12.5\%$.

in bare ions without an IC branch. The details of R, N_γ, and H are summarized below.

Using the SCM discussed in this work, $R(^{100m}\mathrm{Sn})$ can be reasonably estimated. Noting that the excited states of ^{100}Sn must involve core excitations, the weighted average of $R_{\mathrm{exp}}/R_{\mathrm{theo}}$ from the core-excited isomers in ^{98}Cd [21] and ^{96}Ag [20] was used to calculate $R(^{100m}\mathrm{Sn})$. The isomer's spin was assumed to be 6^+, yielding $R = 25\%$. The alternative assumption of the isomer's spin being 8^+ results in $R = 19\%$. In acknowledging the crudeness of the SCM and the possibility of the 8^+ isomer, two additional fractions of 12.5% and 50% were also considered. Then $N_\gamma = 3.57$ was assumed, which is the 2σ upper limit of zero observations in Poisson statistics [69]. Finally, the apparent half-life of the $E2$ isomer during ^{100}Sn's flight through the separator is increased by the factor H, where the T_F was 610(20) ns in the rest frame of ^{100}Sn. The additional H coupled to N_γ in Eq. (6) corresponds to the loss in expected γ-ray counts owing to the IC branch, which was activated the moment the bare ^{100}Sn nuclei were deionized in WAS3ABi during implantation.

Figure 10 shows the $T_{1/2}$ upper limits of the hypothetical isomer in ^{100}Sn as a function of the γ-ray energy and R, where the former affects ϵ and H. The theoretical $B(E2)$ range was relaxed from 0.7–1.1 W.u. to 0.3–2.0 W.u. to generate more conservative limits. For an $E2$ transition in ^{100}Sn, 1 W.u. is 27.57 $e^2\,\mathrm{fm}^4$. For $R = 12.5\%$, the $T_{1/2}$ upper limit line intersects the $B(E2)$ band at approximately 125 keV (minimum energy) and 210 ns (maximum time). Thus, the limits on the hypothetical $E2$ isomer's properties are $E_\gamma > 125$ keV, $\alpha < 0.723$, and $T_{1/2} < 210$ ns. Additional $T_{1/2}$ limits could be generated from the nonobservation of other γ rays in the decay cascade, where the theoretical γ-ray energies for the $4^+ \to 2^+$ and the $2^+ \to 0^+$ transitions are 0.4(1) and 4(1) MeV, respectively [32–34]. Conservative estimates were obtained by minimizing H, ϵ, and R in Eq. (6) within reasonable limits. In this case the first H in Eq. (6), dependent on the isomeric $6^+ \to 4^+$ γ-ray energy, differs from the second H, which depends on the cascading γ-ray energy. $T_{1/2}$ upper limits of 210(20) ns and 0.9(4) μs were obtained based on the two aforementioned hypothetical γ-ray energies, which are consistent with the value estimated from the properties of the delayed low-energy transition. If the isomer has $b_p > 0$, then the partial half-life limit of the electromagnetic decay would increase. Consequently, in view of Fig. 10 the lower limit on the $E2$ γ-ray energy will decrease with increasing b_p.

IV. SUMMARY AND CONCLUSIONS

Half-life and energy measurements of γ-decaying isomers in the ^{100}Sn region were carried out. The results agree well with literature values, and several half-lives were measured with better precision. New results include a 55-keV $E2$ γ ray in ^{92}Rh and a new (4^+) isomeric state; a 44-keV γ ray in ^{96}Ag, confirmed as the $(15^+) \to (13^+)$ $E2$ transition; and $T_{1/2} = 13(2)$ ns for the (6^+) state in ^{98}Cd. These new findings are consistent with shell-model calculations with the SLGM interactions in the pg model space. In addition, a large set of experimental isomeric ratios for nuclei in the vicinity of ^{100}Sn was compared with theoretical values based on the statistical abrasion-ablation model and the SCM. R_{exp} could be reproduced within a factor of 2 for almost all isomers, and discrepancies could be attributed to nuclear structure effects. From realistic isomeric ratio predictions and shell-model calculations, limits are placed on the electromagnetic transition properties of a hypothetical $E2$ isomer in ^{100}Sn: $E_\gamma > 125$ keV, $\alpha < 0.723$, and $T_{1/2} < 210$ ns. The isomeric ratio of the (6^+) isomer in ^{100}Sn was predicted to be 25% for a 345 MeV/u ^{124}Xe primary beam. These constraints will be useful in designing future experiments to probe the excited states of ^{100}Sn.

ACKNOWLEDGMENTS

The authors would like to thank the personnel at the RIKEN Nishina Center for providing the exotic radioactive isotope beam with record intensities. This experiment was performed at RI Beam Factory operated by RIKEN Nishina Center and CNS, University of Tokyo. We acknowledge the EUROBALL Owners Committee for loaning the germanium detectors and the PreSpec Collaboration for the readout electronics of the cluster detectors of EURICA. Support for the WAS3ABi setup was provided by the Rare Isotope Science Project, funded by the Ministry of Education, Science and Technology (MEST) and National Research Foundation (NRF) of Korea, as well as KAKENHI (Grant No. 25247045) of Japan Society for the Promotion of Science (JSPS). The authors acknowledge the support of the DFG cluster of excellence "Origin and Structure of the Universe," German BMBF under Contract No. 05P15PKFNA and the Spanish Ministerio de Economía y Competitividad via Project No. FPA2014-57196-C5-4-P. Part of the research was funded by the Natural Sciences and Engineering Research Council (NSERC) of Canada and also supported by FJNSP LIA (French-Japanese International Associated Laboratory for Nuclear Structure Problems).

[1] C. B. Hinke *et al.*, Nature (London) **486**, 341 (2012).
[2] B. Cederwall *et al.*, Nature (London) **469**, 68 (2011).
[3] B. S. Nara Singh *et al.*, Phys. Rev. Lett. **107**, 172502 (2011).
[4] R. K. Wallace and S. E. Woosley, Astrophys. J. Suppl. **45**, 389 (1981).
[5] H. Schatz, A. Aprahamian, V. Barnard, L. Bildsten, A. Cumming, M. Ouellette, T. Rauscher, F. K. Thielemann, and M. Wiescher, Phys. Rev. Lett. **86**, 3471 (2001).
[6] T. Faestermann, M. Górska, and H. Grawe, Prog. Part. Nucl. Phys. **69**, 85 (2013).
[7] H. Grawe *et al.*, Eur. Phys. J. A **27**, 257 (2006).
[8] O. Häusser *et al.*, Nucl. Phys. A **293**, 248 (1977).
[9] E. Nolte and H. Hick, Z. Phys. A **305**, 289 (1982).
[10] H. Grawe and H. Haas, Phys. Lett. B **120**, 63 (1983).
[11] M. Gorska *et al.*, Phys. Rev. Lett. **79**, 2415 (1997).
[12] J. Doring, H. Grawe, K. Schmidt, R. Borcea, S. Galanopoulos, M. Gorska, S. Harissopulos, M. Hellstrom, Z. Janas, R. Kirchner, M. LaCommara, C. Mazzocchi, E. Roeckl, and R. Schwengner, Phys. Rev. C **68**, 034306 (2003).
[13] M. La Commara *et al.*, Nucl. Phys. A **708**, 167 (2002).
[14] C. Plettner *et al.*, Nucl. Phys. A **733**, 20 (2004).
[15] I. Mukha, L. Batist, E. Roeckl, H. Grawe, J. Doring, A. Blazhev, C. R. Hoffman, Z. Janas, R. Kirchner, M. LaCommara, S. Dean, C. Mazzocchi, C. Plettner, S. L. Tabor, and M. Wiedeking, Phys. Rev. C **70**, 044311 (2004).
[16] I. Mukha *et al.*, Nature (London) **439**, 298 (2006).
[17] P. J. Davies *et al.*, Phys. Lett. B **767**, 474 (2017).
[18] D. Bazin *et al.*, Phys. Rev. Lett. **101**, 252501 (2008).
[19] G. Lorusso *et al.*, Phys. Rev. C **86**, 014313 (2012).
[20] P. Boutachkov *et al.*, Phys. Rev. C **84**, 044311 (2011).
[21] A. Blazhev *et al.*, Phys. Rev. C **69**, 064304 (2004).
[22] A. Blazhev *et al.*, J. Phys. Conf. Series **205**, 012035 (2010).
[23] F. J. D. Serduke, R. D. Lawson, and D. H. Gloeckner, Nucl. Phys. A **256**, 45 (1976).
[24] R. Gross and A. Frenkel, Nucl. Phys. A **267**, 85 (1976).
[25] A. Amusa and R. D. Lawson, Z. Phys. A **307**, 333 (1982).
[26] J. Blomqvist and L. Rydström, Phys. Scr. **31**, 31 (1985).
[27] I. P. Johnston and L. D. Skouras, Eur. Phys. J. A **11**, 125 (2011).
[28] A. F. Lisetskiy, B. A. Brown, M. Horoi, and H. Grawe, Phys. Rev. C **70**, 044314 (2004).
[29] M. Honma, T. Otsuka, T. Mizusaki, and M. Hjorth-Jensen, Phys. Rev. C **80**, 064323 (2009).
[30] A. P. Zuker, A. Poves, F. Nowacki, and S. M. Lenzi, Phys. Rev. C **92**, 024320 (2015).
[31] F. Nowacki, Nucl. Phys. A **704**, 223 (2002).
[32] O. Kavatsyuk *et al.*, Eur. Phys. J. A **31**, 319 (2007).
[33] F. Nowacki (private communication).
[34] V. I. Isakov and K. I. Erokhina, Phys. At. Nucl. **65**, 1431 (2002).
[35] H. Suzuki *et al.*, Nucl. Instrum. Methods B **317**, 756 (2013).
[36] N. Fukuda *et al.*, Nucl. Instrum. Methods B **317**, 323 (2013).
[37] T. Kubo *et al.*, Prog. Theor. Exp. Phys. **2012**, 03C003 (2012).
[38] H. Kumagai *et al.*, Nucl. Instrum. Methods A **470**, 562 (2001).
[39] K. Kimura *et al.*, Nucl. Instrum. Methods A **538**, 608 (2005).
[40] O. B. Tarasov and D. Bazin, Nucl. Instrum. Methods B **266**, 4657 (2008).
[41] I. Čeliković *et al.*, Phys. Rev. Lett. **116**, 162501 (2016).
[42] J. Park *et al.*, Phys. Rev. Lett. (unpublished).
[43] S. Nishimura, Prog. Theor. Exp. Phys. **2012**, 03C006 (2012).
[44] P.-A. Söderström *et al.*, Nucl. Instrum. Methods B **317**, 649 (2013).
[45] T. Kibédi *et al.*, Nucl. Instrum. Methods A **589**, 202 (2008).
[46] M. Pfutzner *et al.*, Phys. Rev. C **65**, 064604 (2002).
[47] G. Audi *et al.*, Chin. Phys. C **41**, 030001 (2017).
[48] T. S. Brock *et al.*, Phys. Rev. C **82**, 061309(R) (2010).
[49] A. B. Garnsworthy *et al.*, Phys. Rev. C **80**, 064303 (2009).
[50] S. Myalski *et al.*, Acta Phys. Pol. B **38**, 1277 (2007).
[51] M. Vencelj *et al.*, Balk. Phys. Lett. Special Issue, p. 298 (2000).
[52] N. Braun, Ph.D. thesis, University of Cologne, Cologne, Germany, 2012.
[53] R. Grzywacz, AIP Conf. Proc. **455**, 430 (1998).
[54] B. A. Brown and W. D. M. Rae, Nucl. Data Sheets **120**, 115 (2014).
[55] D. Rudolph, Nucl. Phys. A **587**, 181 (1995).
[56] D. Abriola and A. A. Sonzogni, Nucl. Data Sheets **107**, 2423 (2006).
[57] C. M. Baglin, Nucl. Data Sheets **113**, 2187 (2012).
[58] D. Kast *et al.*, Z. Phys. A **356**, 363 (1997).
[59] O. L. Pechenaya, C. J. Chiara, D. G. Sarantites, W. Reviol, R. J. Charity, M. P. Carpenter, R. V. F. Janssens, T. Lauritsen, C. J. Lister, D. Seweryniak, S. Zhu, L. L. Andersson, E. K. Johansson, and D. Rudolph, Phys. Rev. C **76**, 011304(R) (2007).
[60] R. Machleidt, Phys. Rev. C **63**, 024001 (2001).
[61] M. Hjorth-Jensen, T. T. S. Kuo, and E. Osnes, Phys. Rep. **261**, 125 (1995).
[62] B. Singh and Z. Hu, Nucl. Data Sheets **98**, 335 (2003).
[63] A. Płochocki *et al.*, Z. Phys. A **342**, 43 (1992).
[64] M. Hjorth-Jensen (private communication).
[65] J. M. Daugas, R. Grzywacz, M. Lewitowicz, M. J. Lopez-Jimenez, F. deOliveira-Santos, J. C. Angelique, L. Axelsson, C. Borcea, C. Longour, and G. Neyens, Phys. Rev. C **63**, 064609 (2001).
[66] K. A. Gladnishki *et al.*, Phys. Rev. C **69**, 024617 (2004).
[67] J.-J. Gaimard and K.-H. Schmidt, Nucl. Phys. A **531**, 709 (1991).
[68] M. de Jong, A. V. Ignatuyk, and K.-H. Schmidt, Nucl. Phys. A **613**, 435 (1997).
[69] K.-H. Schmidt *et al.*, Z. Phys. A **316**, 19 (1984).